

Two Photon Decays of η_c from Lattice QCD

Ting Chen,¹ Ying Chen,² Ming Gong,² Yu-Hong Lei,¹ Ning Li,³ Chuan Liu,^{4,5,*} Yu-Bin Liu,⁶ Zhaofeng Liu,² Jian-Ping Ma,⁷ Wei-Feng Qiu,² Zhan-Lin Wang,¹ and Jian-Bo Zhang⁸
(CLQCD Collaboration)

¹*School of Physics, Peking University, Beijing 100871, China*

²*Institute of High Energy Physics, Chinese Academy of Sciences, Beijing 100049, China*

³*School of Science, Xi'an Technological University, Xi'an 710032, China*

⁴*School of Physics and Center for High Energy Physics, Peking University, Beijing 100871, China*

⁵*Collaborative Innovation Center of Quantum Matter, Beijing 100871, China*

⁶*School of Physics, Nankai University, Tianjin 300071, China*

⁷*Institute of Theoretical Physics, Chinese Academy of Sciences, Beijing 100190, China*

⁸*Department of Physics, Zhejiang University, Hangzhou 311027, China*

We present an exploratory lattice study for the two-photon decay of η_c using $N_f = 2$ twisted mass lattice QCD gauge configurations generated by the European Twisted Mass Collaboration. Two different lattice spacings of $a = 0.067\text{fm}$ and $a = 0.085\text{fm}$ are used in the study, both of which are of physical size of 2fm . The decay widths are found to be $1.025(5)\text{KeV}$ for the coarser lattice and $1.062(5)\text{KeV}$ for the finer lattice respectively where the errors are purely statistical. A naive extrapolation towards the continuum limit yields $\Gamma \simeq 1.122(14)\text{KeV}$ which is smaller than the previous quenched result and most of the current experimental results. Possible reasons are discussed.

I. INTRODUCTION

Charmonium systems play a major role in the understanding of the foundation of quantum chromodynamics (QCD), the fundamental theory for the strong interaction. Due to its intermediate energy scale and the special features of QCD, both perturbative and non-perturbative physics show up within charmonium physics, making it an ideal testing ground for our understanding of QCD from both sides.

Two-photon decay width of η_c has been attracting considerable attention over the years from both theory and experiment sides. For example, it is related to the process $gg \rightarrow \eta_c$ relevant for charmonia production at Large Hadron Collider (LHC) and the small- x gluon distribution function from the inclusive production of η_c which describes the non-leptonic B mesons decays [1]. Furthermore, two-photon branching fraction for charmonium provides a probe for the strong coupling constant at the charmonium scale via the two-photon decay widths, which can be utilized as a sensitive test for the corrections for the non-relativistic approximation in the quark models or the effective field theories such as non-relativistic QCD (NRQCD).

On the experimental side, considerable progress has been made in recent years in the physics of charmonia via the investigations from Belle, BaBar, CLEO-c and BES [2–5]. Two methods can be utilized to measure the two-photon branching fraction for charmonium. One is reconstructing the charmonium in light hadrons with two-photon fusion at e^+e^- machines. The other one is to make $p\bar{p}$ pairs annihilated to charmonium with decay

and then to detect the real $\gamma\gamma$ pairs. Improvements of the measurement for two-photon branching fraction of charmonia will soon be reached in the future.

On the theoretical side, charmonium electromagnetic transitions have been investigated using various theoretical methods [6–14]. In principle, these processes involve both electromagnetic and strong interactions, the former being perturbative in nature while the latter being non-perturbative. Therefore, the study for charmonium transitions requires non-perturbative theoretical methods such as lattice QCD. Normal hadronic matrix element computations are standard in lattice QCD, however, processes involving initial or final photons are a bit more subtle. Since photons are not QCD eigenstates, one has to rely on perturbative methods to “replace” the photon states by the corresponding electromagnetic currents that they couple to. The details of this idea was illustrated in Ref. [15, 16]. Using this technique, the first *ab initio* quenched lattice calculation of two photon decay of charmonia was reported in Ref. [17]. They found a reasonable agreement with the experimental world-average values for η_c and χ_{c0} decay rates. However, an unquenched lattice study is still lacking. In this paper, we would like to fill this gap by exploring the two photon decay rates of η_c meson in lattice QCD with $N_f = 2$ flavors of light quarks in the sea. The gauge configurations utilized in this study are generated by the European Twisted Mass Collaboration (ETMC) [18–29], where the twisted mass fermion parameters are set at the maximal twist. This ensures the so-called automatic $\mathcal{O}(a)$ improvement for on-shell observables where a is the lattice spacing [30].

This paper is organized as follows. In Section II, we briefly review the calculation strategies for the matrix element for two-photon decay of η_c . The matrix element is normally parameterized using a form factor, which in turn is directly related to the double photon decay rates.

* Corresponding author. Email: liuchuan@pku.edu.cn

The following section III are divided into three parts containing details of the simulation: In section III A, we introduce the twist mass fermion formulation and give the parameters of the lattices used in our simulation. In section III C, the continuum and lattice dispersion relations for η_c are checked. In section III E, numerical results of the form factor are presented which are then converted to the decay width of η_c meson. Our final number comes out to be smaller than the world-average experimental result and barely agrees with the previous quenched result. Possible reasons are discussed for this discrepancy. In Section IV, we discuss possible extensions of this cal-

culuation in the future and conclude.

II. STRATEGIES FOR THE COMPUTATION

In this section, we briefly recapitulate the methods for the calculation of two-photon decay rate of η_c presented in Ref. [17]. The amplitude for two-photon decay of η_c can be expressed in terms of a photon two-point function in Minkowski space by means of the Lehmann-Symanzik-Zimmermann (LSZ) reduction formula,

$$\langle \gamma(q_1, \lambda_1) \gamma(q_2, \lambda_2) | \eta_c(p) \rangle = - \lim_{\substack{q'_1 \rightarrow q_1 \\ q'_2 \rightarrow q_2}} \epsilon_\mu^*(q_1, \lambda_1) \epsilon_\nu^*(q_2, \lambda_2) q_1'^2 q_2'^2 \int d^4x d^4y e^{iq'_1 \cdot y + iq'_2 \cdot x} \langle \Omega | T \{ A^\mu(y) A^\nu(x) \} | \eta_c(p_f) \rangle. \quad (1)$$

Here $|\Omega\rangle$ designates the QCD vacuum state, $|\eta_c(p)\rangle$ is the state with an η_c meson of four-momentum p and $|\gamma(q_i, \lambda_i)\rangle$ for $i = 1, 2$ denotes a single photon state with corresponding polarization vector $\epsilon(q_i, \lambda_i)$, with q_i and λ_i being the corresponding four-momentum and helic-

ity, respectively. Then one utilizes the perturbative nature of the photon-quark coupling to approximately integrate out the photon fields and rewrites the corresponding path-integral as,

$$\int \mathcal{D}A \mathcal{D}\bar{\psi} \mathcal{D}\psi e^{iS_{QED}[A, \bar{\psi}, \psi]} A^\mu(y) A^\nu(x) = \int \mathcal{D}A \mathcal{D}\bar{\psi} \mathcal{D}\psi e^{iS_0[A, \bar{\psi}, \psi]} \left(\dots + \frac{e^2}{2} \int d^4z d^4w \right. \\ \left. \times [\bar{\psi}(z) \gamma^\rho \psi(z) A_\rho(z)] [\bar{\psi}(w) \gamma^\sigma \psi(w) A_\sigma(w)] + \dots \right) A^\mu(y) A^\nu(x). \quad (2)$$

The integration over the photon fields can be carried out by Wick contracting the fields into propagators. Neglect-

ing the disconnected diagrams, one arrives at the following equation,

$$\langle \gamma(q_1, \lambda_1) \gamma(q_2, \lambda_2) | \eta_c(p) \rangle = (-e^2) \lim_{\substack{q'_1 \rightarrow q_1 \\ q'_2 \rightarrow q_2}} \epsilon_\mu^*(q_1, \lambda_1) \epsilon_\nu^*(q_2, \lambda_2) q_1'^2 q_2'^2 \int d^4x d^4y d^4w d^4z e^{iq'_1 \cdot y + iq'_2 \cdot x} D^{\mu\rho}(y, z) D^{\nu\sigma}(x, w) \\ \times \langle \Omega | T \{ j_\rho(z) j_\sigma(w) \} | \eta_c(p_f) \rangle. \quad (3)$$

In this equation,

$$D^{\mu\nu}(y, z) = -ig^{\mu\nu} \int \frac{d^4k}{(2\pi)^4} \frac{e^{-ik \cdot (y-z)}}{k^2 + i\epsilon}, \quad (4)$$

is the free photon propagator, which in momentum space will cancel out the inverse propagators outside the integral in Eq. (1) and Eq. (3) when the limit is taken. Effectively, each initial/final photon state in the problem is replaced by a corresponding electromagnetic current operator which couples to the photon and eventually one needs to compute a three-point function of the

form $\langle \Omega | T \{ j_\rho(z) j_\sigma(w) \} | \eta_c(p_f) \rangle$. This quantity is non-perturbative in nature and should be computed using lattice QCD methods.

The current operators such as $j_\rho(x)$ appearing in Eq. (3) are electromagnetic current operators due to all flavors of quarks. However, we will only consider the charm quark in this preliminary study. Contributions due to other quark flavors, e.g. up, down or strange, only come in via disconnected diagrams which are neglected in this exploratory study. Another subtlety in the lattice computation is that, with $c(x)/\bar{c}(x)$ being the bare

charm/anti-charm quark field on the lattice, composite operators such as the current $j_\rho(x) = Z_V(g_0^2)\bar{c}(x)\gamma_\rho c(x)$ needs an extra multiplicative renormalization factor Z_V which we infer from Ref. [31]. To be specific, for the two set of lattices used in this study, the values of the renormalization factor $Z_V(g_0^2)$ are 0.6103(3) and 0.6451(3) for the lattice size $24^3 \times 48$ at $\beta = 3.9$ and $32^3 \times 64$ at $\beta = 4.05$, respectively. Annihilation diagrams of the charm quark itself are also neglected due to OZI-suppression. In fact, in our twisted mass lattice setup, we introduce two different charm quark fields with degenerate masses, so that this type of diagram is absent, see subsection III A.

The resulting expression (3) can then be analytically continued from Minkowski to Euclidean space. This continuation works as long as none of the q_i^2 is too time-like. To be precise, the continuation is fine as long as the virtualities of the two photons $Q_i^2 \equiv (-q_i^2) > -M_V^2$ where M_V is the mass of the lightest vector meson in QCD [15, 17]. For quenched lattice QCD, the lightest vector meson is J/ψ . However, for our unquenched study, it is safe to take $M_V = m_\rho$, i.e. the mass of the ρ meson. Using suitable interpolating operator (denoted by $\mathcal{O}_{\eta_c}(x)$) to create an η_c meson from the vacuum and reversing the operator time-ordering for later convenience, we finally obtain,

$$\langle \eta_c(p_f) | \gamma(q_1, \lambda_1) \gamma(q_2, \lambda_2) \rangle = \lim_{t_f - t \rightarrow \infty} e^2 \frac{\epsilon_\mu(q_1, \lambda_1) \epsilon_\nu(q_2, \lambda_2)}{\frac{Z_{\eta_c}(\mathbf{p}_f)}{2E_{\eta_c}(\mathbf{p}_f)} e^{-E_{\eta_c}(\mathbf{p}_f)(t_f - t)}} \int dt_i e^{-\omega_1 |t_i - t|} \left\langle \Omega \left| T \left\{ \int d^3\mathbf{x} e^{-i\mathbf{p}_f \cdot \mathbf{x}} \mathcal{O}_{\eta_c}(\mathbf{x}, t_f) \int d^3\mathbf{y} e^{i\mathbf{q}_2 \cdot \mathbf{y}} j^\nu(\mathbf{y}, t) j^\mu(\mathbf{0}, t_i) \right\} \right| \Omega \right\rangle, \quad (5)$$

where $\mathcal{O}_{\eta_c}(x)$ is an interpolating operator that will create an η_c meson from the vacuum and ω_1 is the energy of the first photon. The kinematics in this equation is such that four-momentum conservation $p_f = q_1 + q_2$ is valid. This equation serves as the starting point for our subsequent lattice computation. Basically, the current that couples to the first photon is placed at the source time-slice t_i , the second current is at t while the final η_c meson is at the sink time-slice t_f and we are led to the computation of a three-point function of the form

$\langle \Omega | \mathcal{O}_{\eta_c}(\mathbf{x}, t_f) j^\nu(\mathbf{y}, t) j^\mu(\mathbf{0}, t_i) | \Omega \rangle$. Of course, one has to compute the above three-point functions for each t_i and perform an integration (summation) over t_i .

Apart from the above mentioned three-point functions, we also need information from η_c two-point function. For example, in the above equation, $Z_{\eta_c}(p_f)$ is the spectral weight factor while $E_{\eta_c}(p_f)$ is the energy for η_c with four-momentum $p_f = (E_{\eta_c}, \mathbf{p}_f)$. These can be inferred from the corresponding two-point functions for η_c . For this purpose, two-point correlation functions for the interpolating operators \mathcal{O}_{η_c} are computed in the simulation:

$$C(\mathbf{p}_f; t) \equiv \sum_{\mathbf{x}} e^{-i\mathbf{p}_f \cdot \mathbf{x}} \langle \Omega | \mathcal{O}_{\eta_c}(\mathbf{x}, t) \mathcal{O}_{\eta_c}^\dagger(\mathbf{0}, 0) | \Omega \rangle \xrightarrow{t \gg 1} \frac{Z_{\eta_c}(\mathbf{p}_f)^2}{E_{\eta_c}(\mathbf{p}_f)} e^{-E_{\eta_c}(\mathbf{p}_f) \cdot \frac{T}{2}} \cosh \left[E_{\eta_c}(\mathbf{p}_f) \cdot \left(\frac{T}{2} - t \right) \right], \quad (6)$$

where $Z_{\eta_c}(\mathbf{p}_f) = \langle \Omega | \mathcal{O}_{\eta_c} | \eta_c(\mathbf{p}_f) \rangle$ is the corresponding overlap matrix element.

The three-point functions, denoted by $G_{\mu\nu}(t_i, t)$, that need to be computed in our simulation are of the form,

$$G_{\mu\nu}(t_i, t) = \left\langle \Omega \left| T \left\{ \int d^3\mathbf{x} e^{-i\mathbf{p}_f \cdot \mathbf{x}} \mathcal{O}_{\eta_c}(\mathbf{x}, t_f) \int d^3\mathbf{y} e^{i\mathbf{q}_2 \cdot \mathbf{y}} j^\nu(\mathbf{y}, t) j^\mu(\mathbf{0}, t_i) \right\} \right| \Omega \right\rangle. \quad (7)$$

Keeping the sink of η_c fixed at $t_f = T/2$, we compute $G_{\mu\nu}(t_i, t)$ across the temporal direction for all t_i and t on our lattices. For a fixed t_i , one has to use sequential source technique to obtain the t dependence of the three-point function. Then, the same calculation is repeated with a varying t_i . Then, according to Eq. (5), the

desired matrix element is obtained by using the results of $G_{\mu\nu}(t_i, t)$ for different combinations of t_i and t and integrate over t_i with an exponential weight $e^{-\omega_1 |t_i - t|}$. In practice, the integral is replaced by a summation over t_i . To explore the validity of this replacement, we have checked the behavior of the integrand some of which are

illustrated in Fig. 1. It is seen that these integrand as a function of t_i indeed peak around the corresponding t values.

The matrix element $\langle \eta_c | \gamma(q_1, \lambda_1) \gamma(q_2, \lambda_2) \rangle$ can be parameterized using the form factor $F(Q_1^2, Q_2^2)$ as follows,

$$\langle \eta_c | \gamma(q_1, \lambda_1) \gamma(q_2, \lambda_2) \rangle = 2\left(\frac{2}{3}e\right)^2 m_{\eta_c}^{-1} F(Q_1^2, Q_2^2) \epsilon_{\mu\nu\rho\sigma} \times \epsilon^\mu(q_1, \lambda_1) \epsilon^\nu(q_2, \lambda_2) q_1^\rho q_2^\sigma, \quad (8)$$

where $\epsilon^\mu(q_1, \lambda_1), \epsilon^\nu(q_2, \lambda_2)$ are the polarization vectors of the photons while q_1 and q_2 are the corresponding four-momenta. The physical on-shell decay width Γ for η_c to two photons is related to the form factor at $Q_1^2 = Q_2^2 = 0$, which will be referred to as the physical point in the following, via

$$\Gamma = \pi \alpha_{em}^2 \left(\frac{16}{81}\right) m_{\eta_c} |F(0, 0)|^2, \quad (9)$$

where $\alpha_{em} \simeq (1/137)$ is the fine structure constant. Therefore, to extract the physical decay width, we simply compute the corresponding three-point functions in Eq. (5) and then extract the form factors $F(Q_1^2, Q_2^2)$ at various virtualities close to the physical point. Then, we can extract the information for $F(0, 0)$ yielding the physical decay width. Although the physical decay width is only related to $F(0, 0)$, the behavior of $F(Q_1^2, Q_2^2)$ at non-zero virtualities are also of physical relevance when studying processes involving one or two virtual photons.

III. SIMULATION DETAILS

A. Simulation setup

In this study, we use twisted mass fermions at the maximal twist. The most important advantage of this setup is the so-called automatic $\mathcal{O}(a)$ improvement for the physical quantities. To be specific, we use $N_f = 2$ (degenerate u and d quark) twisted mass gauge field configurations generated by the European Twisted Mass Collaboration (ETMC). The other quark flavors, namely strange and charm quarks, are quenched. These quenched flavors are introduced as valence quarks using the Osterwalder-Seiler (OS) type action [18, 32]. Following the Refs. [18, 22, 23], in the valence sector we introduce three twisted doublets, (u, d) , (s, s') and (c, c') with masses μ_l, μ_s and μ_c , respectively. Within each doublet, the two valence quarks are regularized in the physical basis with Wilson parameters of opposite signs ($r = -r' = 1$). The fermion action for the valence sector reads

$$S = (\bar{\chi}_u, \bar{\chi}_d) (D_W + m_{crit} + i\mu_l \gamma_5 \tau_3) \begin{pmatrix} \chi_u \\ \chi_d \end{pmatrix} + (\bar{\chi}_s, \bar{\chi}_{s'}) (D_W + m_{crit} + i\mu_s \gamma_5 \tau_3) \begin{pmatrix} \chi_s \\ \chi_{s'} \end{pmatrix} + (\bar{\chi}_c, \bar{\chi}_{c'}) (D_W + m_{crit} + i\mu_c \gamma_5 \tau_3) \begin{pmatrix} \chi_c \\ \chi_{c'} \end{pmatrix}. \quad (10)$$

One can perform a chiral twist to transform the quark fields in physical basis to the so-called twisted basis as follows:

$$\begin{pmatrix} u \\ d \end{pmatrix} = \exp(i\omega \gamma_5 \tau_3 / 2) \begin{pmatrix} \chi_u \\ \chi_d \end{pmatrix} \\ \begin{pmatrix} s \\ s' \end{pmatrix} = \exp(i\omega \gamma_5 \tau_3 / 2) \begin{pmatrix} \chi_s \\ \chi_{s'} \end{pmatrix} \\ \begin{pmatrix} c \\ c' \end{pmatrix} = \exp(i\omega \gamma_5 \tau_3 / 2) \begin{pmatrix} \chi_c \\ \chi_{c'} \end{pmatrix} \quad (11)$$

where $\omega = \pi/2$ implements the full twist.

Two sets of gauge field ensembles are utilized in this work, each containing 200 gauge field configurations. We shall call them Ensemble I and II respectively. The explicit parameters are listed in Table I. The corresponding renormalization factor $Z_V(g_0^2)$ and the valence charm quark mass parameter μ_c are taken from Ref. [31].

TABLE I. Parameters for the gauge ensembles used in this work. See Ref. [31] and references therein for notations.

Ensemble	β	$a[\text{fm}]$	V/a^4	$a\mu_{\text{sea}}$	$m_\pi[\text{MeV}]$	$a\mu_c$	$Z_V(g_0^2)$
I	3.9	0.085	$24^3 \times 48$	0.004	315	0.215	0.6103(3)
II	4.05	0.067	$32^3 \times 64$	0.003	300	0.185	0.6451(3)

For the meson operators, in the physical basis, we use simple quark bi-linears such as $\bar{q}\Gamma q$ and the corresponding form in twisted basis will be denoted as $\bar{\chi}_q \Gamma' \chi_q$ which can be readily obtained from Eq. (11). For later convenience, these are tabulated in table II together with the possible J^{PC} quantum numbers in the continuum and the names of the corresponding particle in the light and the charm sector. The current operators that appear in Eq. (7) are also listed.

TABLE II. Local interpolating operators for vector and pseudo-scalar states and the current operators that appear in Eq. (7) in both physical and twisted basis, $\bar{q}\Gamma q = \bar{\chi}_q \Gamma' \chi_q$. The names of the corresponding particle and their J^{PC} quantum numbers in the continuum are also listed. The index for i, μ and ν are 1, 2, 3.

	$\rho/J/\psi$	π/η_c	j^μ	j^ν
Γ	γ_i	γ_5	γ_μ	γ_ν
Γ'	γ_i	1	γ_μ	γ_ν
J^{PC}	1^{--}	0^{-+}	1^{--}	1^{--}

B. Twisted boundary conditions

In order to increase the resolution in momentum space, particularly close to the physical point of $Q_1^2 = Q_2^2 = 0$, it is customary to implement the twisted boundary conditions (TBC) [31, 33–35] in recent lattice form factor computations, see e.g. [36]. We have also adopted the

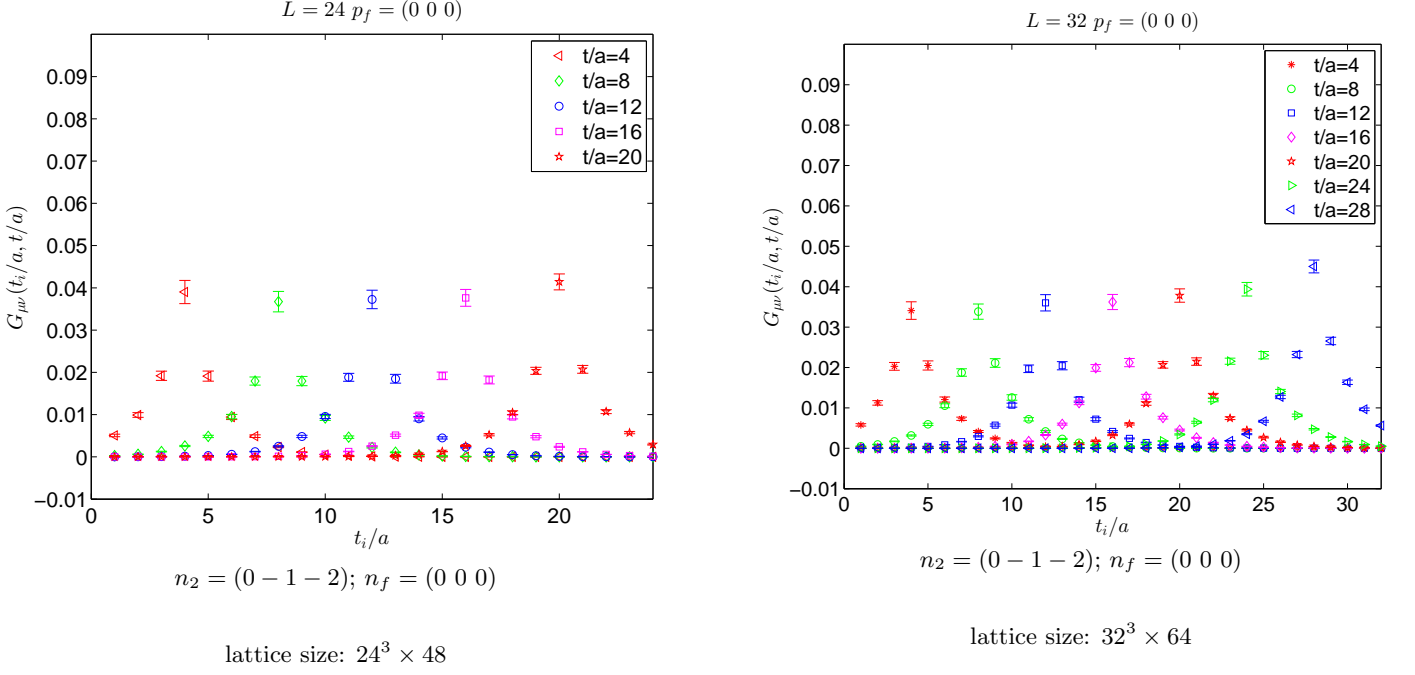


FIG. 1. The integrand in Eq. (5) versus t_i for various insertion points t obtained from our simulation with ensemble I (left panel), and ensemble II (right panel). We take $\mathbf{n}_2 = (0, -1, -2)$; $\mathbf{n}_f = (0, 0, 0)$ in this example. The insertion points are $t = 4, 8, 12, 16, 20$ and $t = 4, 8, 12, 16, 20, 24, 28$ for ensemble I and II, respectively.

twisted boundary conditions for the valence quark fields, also known as partially twisted boundary conditions.

The quark field $\psi_{\boldsymbol{\theta}}(\mathbf{x}, t)$, when it is transported by an amount of L along the spatial direction i ($i = 1, 2, 3$), will change by a phase factor $e^{i\theta_i}$,

$$\psi_{\boldsymbol{\theta}}(\mathbf{x} + L\mathbf{e}_i, t) = e^{i\theta_i} \psi_{\boldsymbol{\theta}}(\mathbf{x}, t), \quad (12)$$

where $\boldsymbol{\theta} = (\theta_1, \theta_2, \theta_3)$ is the twisted angle for the quark field in spatial directions which can be tuned freely. In this calculations, we only twist one of the charm quark field in both vector currents, the other charm quark fields remain un-twisted. If we introduce the new quark fields

$$\hat{c}'(\mathbf{x}, t) = e^{-i\boldsymbol{\theta} \cdot \mathbf{x}/L} c'_{\boldsymbol{\theta}}(\mathbf{x}, t), \quad (13)$$

It is easy to verify that $\hat{c}'(\mathbf{x}, t)$ satisfy the conventional periodic boundary conditions along all spatial directions; i.e., $\hat{c}'(\mathbf{x} + L\mathbf{e}_i, t) = \hat{c}'(\mathbf{x}, t)$ with $i = 1, 2, 3$ if the original field $c'_{\boldsymbol{\theta}}(\mathbf{x}, t)$ satisfies the twisted boundary conditions (12). For Wilson-type fermions, this transformation is equivalent to the replacement of the gauge link; i.e.,

$$U_{\mu}(x) \Rightarrow \hat{U}_{\mu}(x) = e^{i\theta_{\mu}a/L} U_{\mu}(x), \quad (14)$$

for $\mu = 0, 1, 2, 3$ and $\theta_{\mu} = (0, \boldsymbol{\theta})$. In other words, each spatial gauge link is modified by a $U(1)$ -phase. Then the current vectors that appear in Eq. (7) are constructed using the hatted and the original charm quark field as,

$$\begin{cases} j^{\nu}(\mathbf{y}, t) = \bar{c}(\mathbf{y}, t)(\gamma_{\nu})\hat{c}'(\mathbf{y}, t), \\ j^{\mu}(\mathbf{0}, t_i) = \bar{c}'(\mathbf{0}, t_i)(\gamma_{\mu})c(\mathbf{0}, t_i). \end{cases} \quad (15)$$

The allowed momenta on the lattice are thus modified to

$$\mathbf{q}_i = \left(\frac{2\pi}{L}\right) \left(\mathbf{n}_i + \frac{\boldsymbol{\theta}}{2\pi}\right), \quad (16)$$

for $i = 1, 2$ where $\mathbf{n}_i \in \mathbb{Z}^3$ is a three-dimensional integer. By choosing different values for $\boldsymbol{\theta}$, we could obtain more values of \mathbf{q}_1 and \mathbf{q}_2 than conventional periodic boundary conditions. In this paper, apart from the untwisted case of $\boldsymbol{\theta} = (0, 0, 0)$, we have also computed the following cases: $\boldsymbol{\theta} = (0, 0, \pi)$, $(0, 0, \pi/2)$, $(0, 0, \pi/4)$ and $(0, 0, \pi/8)$. These choices offer us many more data points in the vicinity of the physical kinematic region.

C. Meson spectrum and the dispersion relations

Before calculating the matrix element with two photon decay from η_c , the mass for η_c and ρ state and the energy dispersion relations for η_c must be verified. This is particularly important for our study due to the following reasons. Firstly, we use the $N_f = 2$ twisted mass configurations, the sea quarks contains u and d quark field, therefore virtual ρ state can enter the game. Thus, we should calculate the ρ mass so as to ensure the photon virtualities $Q_1^2, Q_2^2 > -m_{\rho}^2$ in this simulations. Secondly, we do need the information from η_c correlation functions, the value of $E_{\eta_c}(\mathbf{p})$ and $Z_{\eta_c}(\mathbf{p})$ in order to extract the relevant matrix elements. Finally, we should also check the dispersion relation of η_c which is quite heavy in lattice units (around 0.95) in our simulation and therefore some

kinematic factors (q_1^ρ and q_2^ρ) that enter Eq.(8) might need modifications accordingly.

Following Eq. (6), the energy $E_{\eta_c}(\mathbf{p}_f)$ for η_c state with three-momentum \mathbf{p}_f can be obtained from the corresponding two-point function via

$$\cosh(E_{\eta_c}(\mathbf{p}_f)) = \frac{C(\mathbf{p}_f; t-1) + C(\mathbf{p}_f; t+1)}{2C(\mathbf{p}_f; t)} \quad (17)$$

The two point function is symmetric about $t = T/2$. In real simulation we average the data from two halves about $t = T/2$ to improve statistics. We use the effective mass plateaus at zero three-momentum for the η_c and ρ state to obtain the masses which are then listed in Table III. The mass of the η_c comes out to be lighter than its physical value since these values are still finite lattice spacing values. When extrapolated towards the continuum limit, the mass will become compatible with the experimental value. The mass of the ρ here serves to restrict our kinematic regions where analytic continuation is justified.

TABLE III. The meson mass values for η_c and ρ obtained from the two ensembles in this work.

Ensemble	$m_{\eta_c} [\text{MeV}]$	$m_\rho [\text{MeV}]$
I	2678(3)	903(88)
II	2812(2)	1051(50)

Similarly, we obtain the energies for η_c at non-vanishing momenta via Eq. (17) which then can be utilized to verify the the following two dispersion relations: the conventional one in the continuum,

$$E^2(\mathbf{p}) = m^2 + Z_{\text{cont}} \cdot \sum_i p_i^2, \quad (18)$$

and its lattice counterpart,

$$4 \sinh^2 \frac{E(\mathbf{p})}{2} = 4 \sinh^2 \frac{m}{2} + Z_{\text{latt}} \cdot 4 \sum_i \sin^2 \left(\frac{p_i}{2} \right). \quad (19)$$

For free particles, the constants Z_{cont} and Z_{latt} should be close to unity. In Fig. 2, we show this comparison for the two dispersion relations of the η_c states in our simulation. In the left/right panel, the dispersion relations are illustrated using continuum/lattice dispersion relations, respectively. In both panels, points with errors are from simulations on $32^3 \times 64$ (open circles) or $24^3 \times 48$ (stars) lattices. Straight lines are the corresponding linear fits to the data. It is seen that, although both dispersion relations can be fitted nicely using linear fits, the slope for the naive continuum dispersion relation, i.e. Z_{cont} is definitely different from unity while its lattice counterpart Z_{latt} is close. This suggests that, for the η_c state, we should use the lattice dispersion relations instead of the naive continuum dispersion relation. This is not surprising since η_c is quite heavy in lattice units. This modification of the dispersion relation does have consequences on our determination of the form factor.

D. Kinematics

In order to fully explore the form factor close to the physical point $Q_1^2 = Q_2^2 = 0$, we performed a parameter scan in the two virtualities. The following notations will be utilized. First of all, in the continuum, we will use $q_{1,2}$ to designate the four-momentum of the two photons. We will also use $\omega_{1,2}$ to denote the temporal component of $q_{1,2}$, i.e. $\omega_{1,2} \equiv q_{1,2}^0$. When the photons are on-shell, we have $\omega_{1,2} = |\mathbf{q}|_{1,2}$ with $\mathbf{q}_{1,2}$ being the corresponding three-momentum. The so-called virtuality of the photons are defined as the corresponding four-momentum squared: $Q_{1,2}^2 \equiv (-q_{1,2}^2)$.

On the lattice, however, there are also lattice counterparts of the above notations, arising from the lattice dispersion relation (19). For that we simply add a hat on the corresponding variable. For example, we will use $\hat{\omega}_1 = 2 \sinh(\omega_1/2)$ to denote the lattice version of ω_1 .

The computation has to cover the physical interesting kinematic region. For this purpose, we have to scan the corresponding parameter space. We basically follow the following strategy: We first fix the four-momentum of η_c , $p_f = (E_{\eta_c}, \mathbf{p}_f)$, and place it on a given time-slice $t_f = T$. Note that we just have to fix $\mathbf{p}_f = \mathbf{n}_f(2\pi/L)$ and E_{η_c} can be obtained from the dispersion relation (19). This effectively puts η_c on-shell. Here we also have the freedom to pick a value for the twist angle θ . Then, we judiciously choose several values of virtuality Q_1^2 around the physical point $Q_1^2 = 0$. To be specific, we picked the range $Q_1^2 \in [-0.5, +0.5] \text{GeV}^2$, which satisfies the constraint $Q_1^2 > -m_\rho^2$.¹ Since $\mathbf{p}_f = \mathbf{q}_1 + \mathbf{q}_2$, this means that, for a given \mathbf{p}_f , a choice of \mathbf{q}_1 completely specifies \mathbf{q}_2 and vice versa. We therefore take several choices of $\mathbf{q}_1 = \mathbf{n}_1(2\pi/L)$ by changing three-dimensional integer \mathbf{n}_1 . At this stage, we can compute the energy of the first photon ω_1 , since $\omega_1^2 = \mathbf{q}_1^2 - Q_1^2$. It turns out that we can also compute the virtuality of the second photon, $Q_2^2 = |\mathbf{q}_2|^2 - \omega_2^2$, since $\omega_2 = E_{\eta_c} - \omega_1$ and \mathbf{q}_2 is also known by the choice of \mathbf{q}_1 . One has to make sure that, the values of Q_2^2 thus computed do satisfy the constraint $Q_2^2 > -m_\rho^2$ otherwise it is omitted. This procedure is summarized as follows:

1. Pick \mathbf{p}_f and θ . Obtain $E_{\eta_c}(\mathbf{p}_f)$ from dispersion relation (19);
2. Judiciously choose several values of Q_1^2 in a suitable range, say $Q_1^2 \in [-0.5, +0.5] \text{GeV}^2$;
3. Pick values of \mathbf{n}_1 such that $\mathbf{q}_1 = \mathbf{n}_1(2\pi/L)$. This fixes both ω_1 and Q_2^2 , using energy-momentum conservation;
4. Make sure all values of $Q_1^2, Q_2^2 > -m_\rho^2$, otherwise the choice is simply ignored;

¹ This is valid with the physical ρ meson mass. Our lattice values yield a less stringent constraint.

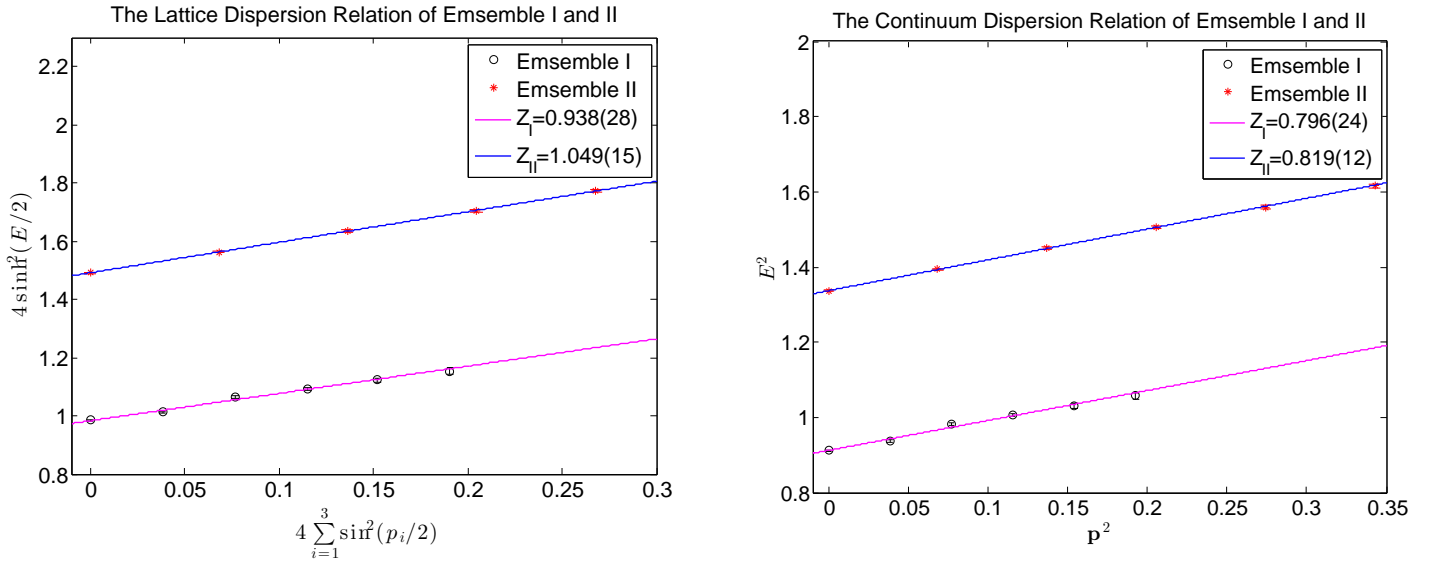


FIG. 2. η_c meson dispersion relation obtained from simulations on Ensemble I (crosses) and Ensemble II (open circles). In the left/right panel, the horizontal axis represents the continuum/lattice three-momentum squared variable. Straight lines in both panels are the corresponding linear fits using continuum/lattice dispersion relations Eq. (18) or Eq. (19). The fitted parameters Z_{cont} and Z_{latt} together with their errors are also shown.

5. For each validated choice above, compute the three-point functions (7), the two-point functions (6) and eventually obtain the hadronic matrix element using Eq. (5).

E. Form factors

In order to compute the desired hadronic matrix element $\langle \eta_c(p_f) | \gamma(q_1, \lambda_1) \gamma(q_2, \lambda_2) \rangle$ in Eq. (5), we choose to place η_c state at a fixed sink position $t_f = T$. This sink position is then used as a sequential source for a backward charm propagator inversion. We compute this with all possible source positions t_i and insertion point t . This method allows us to freely vary the value of ω_1 , Q_1^2 (as discussed in previous subsection) and to directly inspect the behavior of the integrand in Eq. (5).

Taking $\mathbf{p}_f = \mathbf{0}$ for the η_c state as an example,, we show the behavior of the integrand in Fig. 1 for insertion positions $t = 4, 8, 12, 16, 20$ for ensemble I and $t = 4, 8, 12, 16, 20, 24, 28$ for ensemble II. It is seen that the integrand is peaked around $t_i = t$, making the contributions close to this point the dominant part of the matrix element. For the lattice theory, the integration of t_i in Eq. (5) is replaced by a summation.

When passing from the matrix element to the form factors, one should be careful about the form of the momenta to use. Recall that these momentum factors originate from derivatives in the continuum. On the lattice, they should be replaced by the corresponding finite differences, i.e. one should use the lattice version of the momentum: $q^0 \rightarrow 2 \sinh(q^0/2)$ and $q^i \rightarrow 2 \sin(q^i/2)$. Since the spatial momenta that we are using are relatively small

in lattice units, the effect of this replacement might be optional. However, for the 0-th component, since each of the photon is roughly half of the η_c energy which is large in lattice units as we discussed in subsection III C, this replacement does make a difference.

According to Eq. (5), the matrix element and therefore also the form factor $F(Q_1^2, Q_2^2)$ should be independent of the insertion point t . We indeed observe this plateau behavior in our data which is illustrated in Fig. 3 for the case of $Q_1^2 = 0$ as an example. Other cases are similar. Fitting these plateaus then yields the corresponding values for the matrix element $\langle \eta_c | \gamma(q_1, \lambda_1) \gamma(q_2, \lambda_2) \rangle$ or equivalently the form factor $F(Q_1^2, Q_2^2)$.

To describe the virtuality dependence of the form factor, we adopt a simple one-pole parametrization to fit our data.

$$F(Q_1^2, Q_2^2) = F(Q_1^2, 0) / (1 + Q_2^2 / \mu^2(Q_1^2)), \quad (20)$$

where $F(Q_1^2, 0)$ and $\mu^2(Q_1^2)$ are regarded as the fitting parameters at the given value of Q_1^2 . Since measurements at different values of Q_1^2 or Q_2^2 are all obtained on the same set of ensembles, we adopt the correlated fits, taking into account possible correlations among different Q^2 values. The covariance matrix among them are estimated using a bootstrap method.

As an example, taking $Q_1^2 = -0.5 \text{ GeV}^2$, the fitting results are shown in Fig. 4. It is seen that this simple formula describes the data rather well even for quite large values of Q_2^2 . We therefore have taken all available values of Q_2^2 into the fitting process. Notice also that, by using the twisted boundary conditions together with different combinations of the lattice momenta, we are able to populate the physical region close to $Q_1^2 = Q_2^2 = 0$

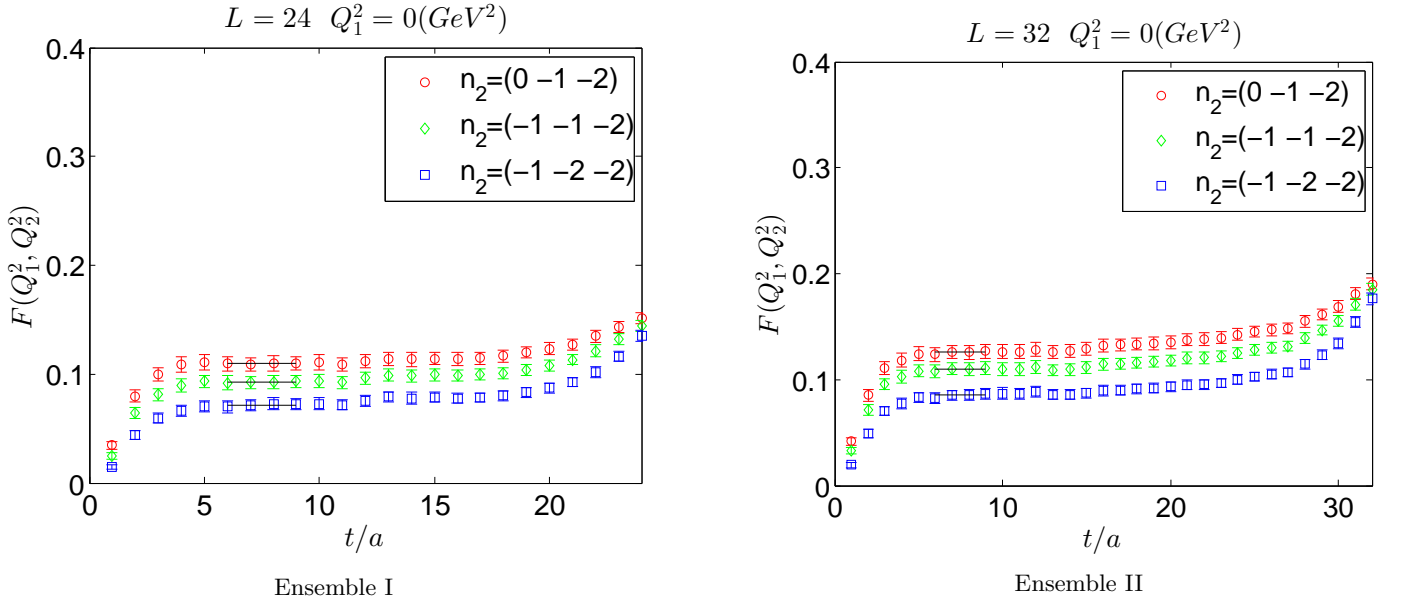


FIG. 3. The plateau of the form factor obtained by an integration (summation) over t_i for three-point function $G_{\mu\nu}(t_i, t)$ with ensemble I (left panel) and ensemble II (right panel). We take $Q_1^2 = 0$; $n_f = (0, 0, 0)$ in this particular plot. Different data points correspond to different choices of \mathbf{n}_2 as indicated.

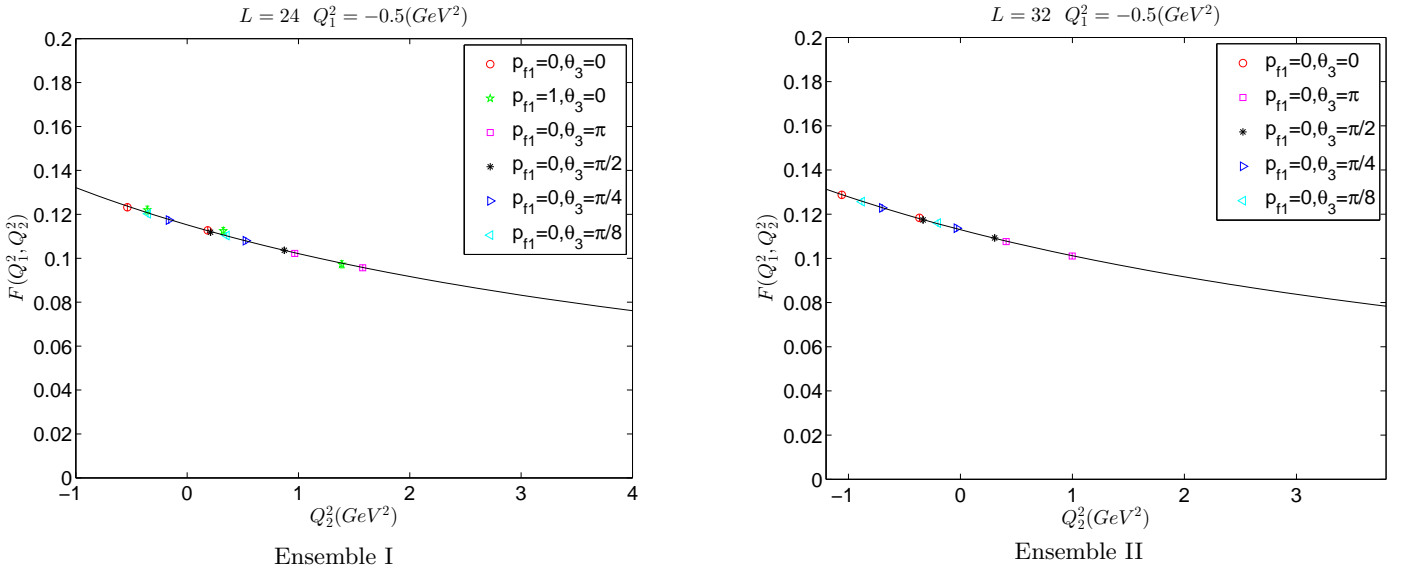


FIG. 4. The fitted results for $F(Q_1^2, Q_2^2) = F(Q_1^2, 0)/(1 + Q_2^2/\mu^2(Q_1^2))$ by one-pole form factor for Ensemble I (left figure) and Ensemble II (right figure) at a fixed value of $Q_1^2 = -0.5 GeV^2$. Different data points correspond to different parameter combinations as indicated in the Figure. p_{f1} denotes x-component of the momentum \mathbf{p}_f of η_c , and θ_3 represents z-component of twisted angle $\boldsymbol{\theta}$.

rather effectively. We have tried both correlated and uncorrelated fits on our data. The central values for the fitted parameters are compatible, however, the error estimates are somewhat different. We adopt the correlated fits as our final results. Fits for other set of parameters are similar and the final results are summarized in Table IV for reference.

Having obtained the results for $F(Q_1^2, 0)$, we can fit it

again with another one-pole form,

$$F(Q_1^2, 0) = F(0, 0)/(1 + Q_1^2/\nu^2). \quad (21)$$

with $F(0, 0)$ and ν^2 being the fitting parameters. This is illustrated in Fig. 5 for two of our ensembles. Again, correlated fits are adopted here.

Apart from fitting the data in a two-step procedure as described above, we have also tried to fit the data in a

TABLE IV. The summary of fitted results for $F(Q_1^2, 0)$ and $\mu^2(Q_1^2)$ using Eq. (20) for Ensemble I (left four columns) and Ensemble II (right four column). The corresponding χ^2/dof are also presented.

Ensemble I				Ensemble II			
$Q_1^2 (GeV^2)$	$F(Q_1^2, 0)$	$\mu^2(Q_1^2) (GeV^2)$	χ^2/dof	$Q_1^2 (GeV^2)$	$F(Q_1^2, 0)$	$\mu^2(Q_1^2) (GeV^2)$	χ^2/dof
-0.5	0.11521(46)	7.79(38)	2.22/11	-0.5	0.11297(44)	8.59(42)	0.27/8
-0.4	0.11353(42)	7.82(36)	2.33/11	-0.4	0.11163(47)	8.62(49)	0.24/7
-0.3	0.11187(39)	7.83(36)	2.30/11	-0.3	0.11031(49)	8.61(54)	0.20/6
-0.2	0.11038(41)	7.83(37)	2.12/10	-0.2	0.10901(52)	8.69(53)	0.19/6
-0.1	0.10874(39)	7.87(36)	2.30/10	-0.1	0.10771(54)	8.62(64)	0.15/5
0	0.10721(43)	7.90(45)	1.79/8	0	0.10645(59)	8.67(59)	0.15/5
0.1	0.10581(46)	7.82(52)	1.37/7	0.1	0.10523(67)	8.74(60)	0.13/5
0.2	0.10432(44)	7.85(49)	1.54/7	0.2	0.10402(71)	8.70(73)	0.03/3
0.3	0.10283(44)	7.92(47)	1.43/7	0.3	0.10191(56)	7.74(47)	2.9/3
0.4	0.10142(45)	7.96(44)	1.51/7	0.4	0.10056(58)	7.83(45)	2.8/3
0.5	0.10012(51)	7.82(51)	0.95/5	0.5	0.09936(63)	7.64(55)	2.3/2

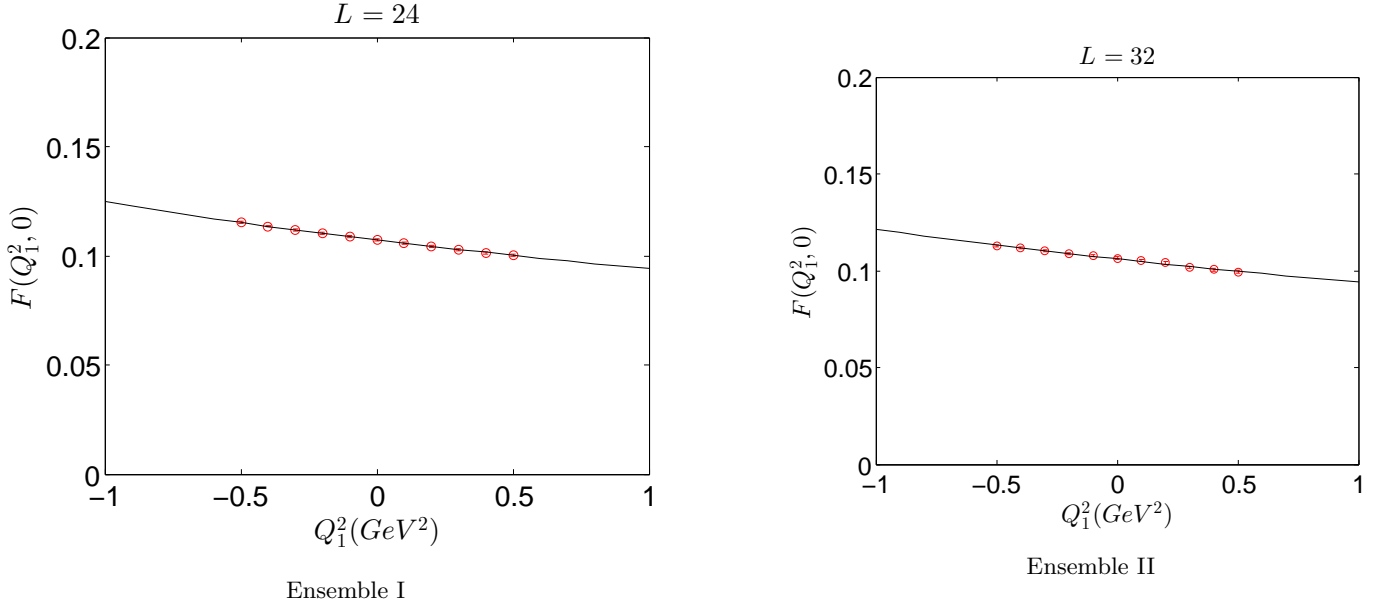


FIG. 5. $F(Q_1^2, 0)$ is again fitted with a one-pole form: $F(Q_1^2, 0) = F(0, 0)/(1 + Q_1^2/\nu^2)$ for Ensemble I (left figure) and Ensemble II (right figure).

one-step method. When we plug Eq. 21 into Eq. 20 and assuming that we are only interested in the value of the form factor close to the physical point, we may Taylor expand it assuming both Q_1^2 and Q_2^2 are small,

$$F(Q_1^2, Q_2^2) = F(0, 0) + aQ_1^2 + bQ_2^2, \quad Q_1^2, Q_2^2 \sim 0 \quad (22)$$

Thus, we could fit the data in a region close to the origin with $F(0, 0)$, a and b being the fitting parameters. This is illustrated in Fig. 6 for two of our ensembles. In each case, 35 data points of (Q_1^2, Q_2^2) close to the origin are taken and the corresponding form factors $F(Q_1^2, Q_2^2)$ are obtained. Then using a linear fit in both Q_1^2 and Q_2^2 , c.f. Eq. (22), the form factors at the origin are obtained for both ensembles. Again, correlated fits are adopted here. The fitting results are summarized in Table VI.

When computing the physical double photon decay width, according to Eq. (9), one has to plug in the mass

of the η_c meson. What we really compute on the lattice is the combination of correlation functions which is related to the matrix element $\langle \eta_c | \gamma(q_1, \lambda_1) \gamma(q_2, \lambda_2) \rangle$ via Eq. (5). When we parameterize this particular matrix element in terms of form factor in Eq. (8), the relation involves m_{η_c} as well. Therefore, the decay width turns out to be proportional to $m_{\eta_c}^3$: $\Gamma \propto m_{\eta_c}^3 |\langle \eta_c | \gamma(q_1, \lambda_1) \gamma(q_2, \lambda_2) \rangle|^2$. Here it is then quite different if one substitutes in the value of m_{η_c} obtained on the lattice, or the true physical value of $m_{\eta_c}^{\text{phys.}} = 2.98 \text{ GeV}$, the two differs by about 10% for the coarser lattice and about 5% for the finer lattice. Therefore, if one would substitute in the true physical mass, it will result in a 15% difference in the value of Γ for the finer lattice and about 30% for the coarser one.

The reason for the above mentioned difference is the following. We are taking the value of the valence charm

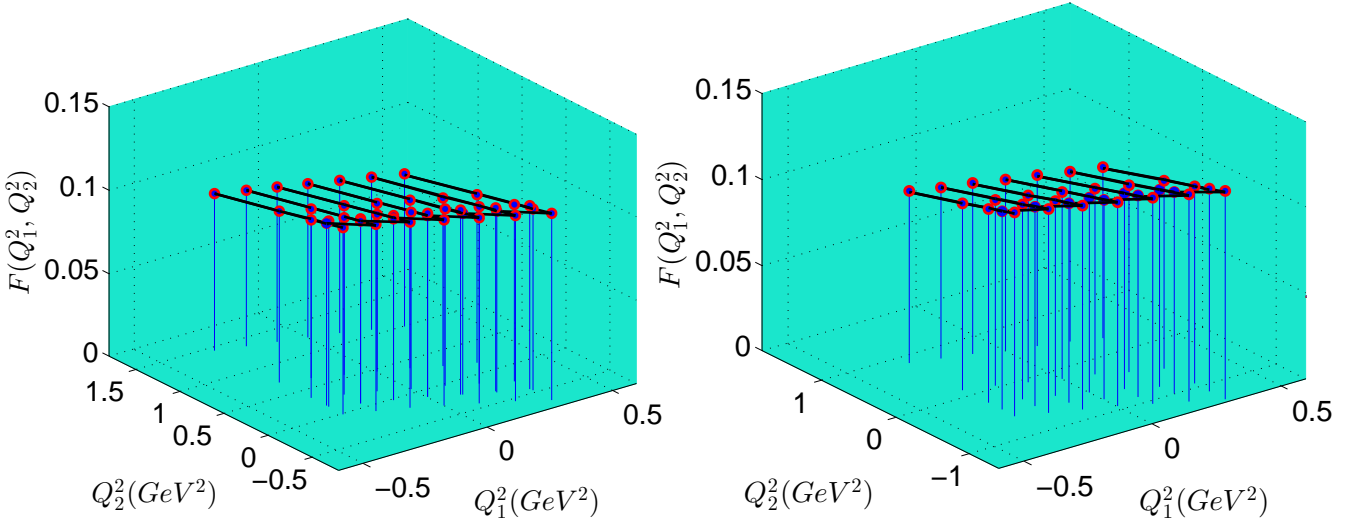


FIG. 6. $F(Q_1^2, Q_2^2)$ is fitted with Eq. (22) are shown for Ensemble I (left figure) and Ensemble II (right figure).

quark mass parameter μ_c from Ref. [31]. There, it is assumed that, when the continuum limit is taken, the value of m_{η_c} will recover its physical value. However, being on a finite lattice, the computed value of m_{η_c} comes out to be less than the corresponding physical value. The difference of the two is in fact an estimate of the finite lattice spacing error. In fact, m_{η_c} is not the only factor which affects the results. The renormalization factor $Z_V(g_0^2)$ that we quoted in Table I also depends on the lattice spacing. Therefore, we think it is more consistent to substitute in the values of m_{η_c} computed on each ensembles. In the end, of course, one should try to take the continuum limit when the lattice computations are performed on a set of ensembles with different lattice spacings.

If using the two-step fitting procedure using Eq. (20) and using Eq. (21), with the values of m_{η_c} obtained from each ensemble substituted in, we obtain for the decay width $\Gamma = 1.019(3)\text{KeV}$ for the coarser and $\Gamma = 1.043(3)\text{KeV}$ for the finer lattice ensembles. These results for the form factor $F(0,0)$ together with the corresponding results for the decay width are summarized in Table V.

As for the one-step fitting procedure using Eq. (22), we obtain $\Gamma = 1.025(5)\text{KeV}$ for the coarser and $\Gamma = 1.062(5)\text{KeV}$ for the finer lattice ensembles. The results for the form factor $F(0,0)$ and $\Gamma(\eta_c \rightarrow \gamma\gamma)$ are consistent with each other for Ensemble I using two different types of fitting procedure. However, for Ensemble II, a combined fitting using Eq. (22) gives a larger result for both $F(0,0)$ and $\Gamma(\eta_c \rightarrow \gamma\gamma)$. We think the value using the combined fit is more reliable since it gives a much less value of χ^2/dof . In the combined fitting, the naive continuum extrapolated result for the decay width reads $\Gamma = 1.122(14)\text{KeV}$. The fitted results for $F(0,0)$ together with the corresponding results for the decay width are summarized in Table VI.

Let us now discuss the possible systematic errors. Al-

though the mass of the pion in the two ensembles are relatively heavy, we do not expect the double photon decay width to be very sensitive to the pion mass. Also, since both of our ensembles have $m_\pi L \sim 3.3$, we do not expect very large finite volume errors as well. Since we have only two ensembles, it is not possible to make reliable extrapolation towards the continuum limit. However, if one would try a naive continuum limit extrapolation, assuming an $\mathcal{O}(a^2)$ error, we obtain $\Gamma = 1.082(10)\text{KeV}$ which is also listed in Table V. There are of course other sources of systematic errors, e.g. the neglecting of the so-called disconnected contributions, the quenching of the strange quark, etc. Therefore, we decided not to quantify the systematic errors in this exploratory study. However, as we discussed above, the difference in the η_c mass already indicates that there might be a finite lattice spacing error at the order of 15% for the finer and 30% for the coarser ensembles, respectively.

Now let us briefly discuss the implications of our lattice results for Γ . First of all, our results are substantially smaller than the previously obtained quenched lattice result in Ref. [17], which we quote: $\Gamma = 2.65(26)_{stat}(80)_{scal.}(53)_{quen.}\text{KeV}$. Second, our value is also much smaller than most of the experimental values. The current experimental value, according to PDG, is about 5.0 KeV with an error of 0.4 KeV [37]. However, one should note that the most recent determination of this quantity by Belle [38] with the result $5.8 \pm 1.1\text{ KeV}$ is not a direct measurement of $\Gamma_{\gamma\gamma}$ itself, but the product $\Gamma_{\gamma\gamma} B(\eta_c \rightarrow \eta' \pi^+ \pi^-) \simeq 50.5\text{ eV}$. Therefore, the value of $\Gamma_{\gamma\gamma}$ is usually extracted by inferring to earlier measurements in other channels, making the final results for $\Gamma_{\gamma\gamma}$ differ quite a bit. For example, if we blindly use the PDG quoted value of the branching ratio, $B(\eta_c \rightarrow \eta' \pi^+ \pi^-) = 0.041 \pm 0.017$, we arrive at $\Gamma_{\gamma\gamma} \simeq 1.25\text{ KeV}$, which is comparable to our lattice result. However, if we would infer $\Gamma_{\gamma\gamma}$ from

TABLE V. $F(Q_1^2, 0)$ is again fitted with a one-pole form: $F(Q_1^2, 0) = F(0, 0)/(1 + Q_1^2/\nu^2)$ are shown for the two ensembles (the first two lines). In the last column, we show the decay width obtained using Eq. (9). A naive continuum extrapolation are shown in the third line for reference.

	$F(0, 0)$	$\nu^2(GeV^2)$	χ^2/dof	$\Gamma(\eta_c \rightarrow \gamma\gamma)(\text{KeV})$
Ensemble I	0.10719(13)	7.13(20)	0.19/9	1.019(3)
Ensemble II	0.10608(17)	7.88(29)	3.4/9	1.043(3)
Naive extrapolation				1.082(10)

TABLE VI. $F(Q_1^2, Q_2^2)$ is fitted with Eq. (22) are shown for the two ensembles (the first two lines). In the last column, we show the decay width obtained using Eq. (9). A naive continuum extrapolation are shown in the third line for reference.

	$F(0, 0)$	a	b	χ^2/dof	$\Gamma(\eta_c \rightarrow \gamma\gamma)(\text{KeV})$
Ensemble I	0.10750(24)	-0.0138(11)	-0.01216(36)	2.67/32	1.025(5)
Ensemble II	0.10705(24)	-0.0124(11)	-0.01282(38)	2.50/32	1.062(5)
Naive extrapolation					1.122(14)

the ratio of $\Gamma_{\gamma\gamma}\Gamma(K\bar{K}\pi)/\Gamma_{tot} = 0.407 \pm 0.027\text{KeV}$ and $\Gamma(K\bar{K}\pi)/\Gamma_{tot} = (7.0 \pm 1.2) \times 10^{-2}$, we end up with $\Gamma_{\gamma\gamma} = 5.8 \pm 1.1\text{KeV}$ as in Ref. [38]. Therefore, it is highly desirable to have a more precise and/or direct measurement of this quantity in future experiments.

The possible reasons for these apparent discrepancies can come from several sources to be discussed below. First, we have used different configurations from the quenched calculations. Our calculation takes into account the sea quark contributions from u and d quarks while in Ref. [17] these have been ignored. Although the quenching errors have been estimated in Ref. [17], it is well-known that this type of systematic is very difficult to quantify accurately. It is therefore quite possible that these effects have been under-estimated in Ref. [17].

Another possibility is that we have a rather large systematic errors which is not fully quantified in this exploratory study. It is seen that our statistical errors seem to be small. However, as mentioned above, we do observe a large finite lattice spacing error of about 15-30% just from the mass of the η_c . Since we have only two lattice spacings, the continuum limit extrapolation is also not well-controlled. In fact, if we blindly ascribe an error of about 15% for the numbers of the decay width for the two ensembles in Table V, it is possible that we could end up with a number that is close to the quenched result but with a rather large error coming from the continuum limit extrapolation. Of course, it is also possible that this disagreement is due to the combination of the above mentioned sources. In any case, a more systematic study with more lattice ensembles will definitely help to clarify these issues.

IV. CONCLUSIONS

In this exploratory study, we calculate the decay width for two-photon decay of η_c using unquenched $N_f = 2$ twisted mass fermion configurations. The computation

is done with two lattice ensembles at two different lattice spacings. The mass spectrum and dispersion relations for the η_c state are first examined. It is verified that lattice dispersion relations are better than the continuum ones. The implication of this is carried over to the computation of hadronic matrix element and the corresponding form factors.

By calculating various three-point functions, two-photon decays of η_c matrix element are obtained at various of virtualities. It is particularly helpful to implement the so-called twisted boundary conditions which enable us to populate the physical region well. The matrix element is decomposed into kinematic factors and one form factor $F(Q_1^2, Q_2^2)$ which is obtained in a region close to the physical point. Then, we adopt a simple one-pole parametrization to fit the data for each value of Q_1^2 , and subsequently fit $F(Q_1^2, 0)$ again with a one-pole form yielding the value of $F(0, 0)$. A naive continuum extrapolation gives $\Gamma = 1.082(10)\text{KeV}$. We also use the Taylor expansion for $F(Q_1^2, Q_2^2)$ with respect to Q_1^2 and Q_2^2 close to the origin and extract the value of $F(0, 0)$, the naive continuum extrapolation of which yields $\Gamma = 1.122(14)\text{KeV}$.

Our result is significantly smaller than both the quenched result and the experimental values quoted by the PDG. However, taking into account of the possibly large systematic errors in the present lattice computations and the large uncertainties in the experimental result itself, it is still premature to say that there is a severe discrepancy here. Obviously, future more systematic lattice studies with various lattice spacings and more statistics are very much welcome here. It would also be helpful to estimate the disconnected contributions that has been neglected in this exploratory study. It will also be helpful to use other types of unquenched configurations, e.g. with $2 + 1$ flavors or even $2 + 1 + 1$ flavors in order to estimate the effects for the quenching of the other quark flavors. Last but not the least, more precise experimental results on double photon decays of charmonium are

crucial in this area as well.

ACKNOWLEDGMENTS

The authors would like to thank the European Twisted Mass Collaboration (ETMC) to allow us to use their gauge field configurations. Our thanks also go to National Supercomputing Center in Tianjin (NSCC) and the Beijing Computing Center (BCC) where part of the numerical computations are performed. This work is supported in part by the National Science Foundation of China (NSFC) under the project No.11505132, No.11335001, No.11275169, No.11405178, No.11105153.

It is also supported in part by the DFG and the NSFC (No.11261130311) through funds provided to the Sino-German CRC 110 “Symmetries and the Emergence of Structure in QCD”. This work is also funded in part by National Basic Research Program of China (973 Program) under code number 2015CB856700. M. Gong and Z. Liu are partially supported by the Youth Innovation Promotion Association of CAS (2013013, 2011013). This work is also supported by the Scientific Research Program Funded by Shaanxi Provincial Education Department under the grant No. 15JK1348, and Natural Science Basic Research Plan in Shaanxi Province of China (Program No. 2016JQ1009).

-
- [1] D. Diakonov, M. G. Ryskin, and A. G. Shuvaev, JHEP **02**, 069 (2013), arXiv:1211.1578 [hep-ph].
 - [2] J. P. Lees et al. (BaBar), Phys. Rev. **D81**, 052010 (2010), arXiv:1002.3000 [hep-ex].
 - [3] T. N. Pham, Nucl. Phys. Proc. Suppl. **234**, 291 (2013).
 - [4] V. Savinov (Belle), Nucl. Phys. Proc. Suppl. **234**, 287 (2013).
 - [5] M. Ablikim et al. (BESIII), Phys. Rev. **D85**, 112008 (2012), arXiv:1205.4284 [hep-ex].
 - [6] P. Guo, T. Ypez-Martnez, and A. P. Szczepaniak, Phys. Rev. **D89**, 116005 (2014), arXiv:1402.5863 [hep-ph].
 - [7] O. Bondareko (BESIII), PoS **QNP2012**, 091 (2012).
 - [8] G. Li and Q. Zhao, Phys. Rev. **D84**, 074005 (2011), arXiv:1107.2037 [hep-ph].
 - [9] Y. Chen et al., Phys. Rev. **D84**, 034503 (2011), arXiv:1104.2655 [hep-lat].
 - [10] U.-G. Meissner, Int. J. Mod. Phys. Conf. Ser. **02**, 56 (2011).
 - [11] C. E. Thomas (Hadron Spectrum), Chin. Phys. **C34**, 1512 (2010).
 - [12] C. E. Thomas (Hadron Spectrum), AIP Conf. Proc. **1257**, 77 (2010).
 - [13] Y.-P. Kuang, T. Barnes, C. Yuan, and H.-X. Chen, Int. J. Mod. Phys. **A24S1**, 327 (2009).
 - [14] J. J. Dudek, R. Edwards, and C. E. Thomas, Phys. Rev. **D79**, 094504 (2009), arXiv:0902.2241 [hep-ph].
 - [15] X.-d. Ji and C.-w. Jung, Phys. Rev. Lett. **86**, 208 (2001), arXiv:hep-lat/0101014 [hep-lat].
 - [16] X.-d. Ji and C.-w. Jung, Phys. Rev. **D64**, 034506 (2001), arXiv:hep-lat/0103007 [hep-lat].
 - [17] J. J. Dudek and R. G. Edwards, Phys. Rev. Lett. **97**, 172001 (2006), arXiv:hep-ph/0607140 [hep-ph].
 - [18] R. Frezzotti and G. C. Rossi, JHEP **10**, 070 (2004), arXiv:hep-lat/0407002 [hep-lat].
 - [19] A. Shindler, Phys. Rept. **461**, 37 (2008), arXiv:0707.4093 [hep-lat].
 - [20] P. Boucaud et al. (ETM), Phys. Lett. **B650**, 304 (2007), arXiv:hep-lat/0701012 [hep-lat].
 - [21] P. Boucaud et al. (ETM), Comput. Phys. Commun. **179**, 695 (2008), arXiv:0803.0224 [hep-lat].
 - [22] B. Blossier et al. (European Twisted Mass), JHEP **04**, 020 (2008), arXiv:0709.4574 [hep-lat].
 - [23] B. Blossier et al. (ETM), JHEP **07**, 043 (2009).
 - [24] R. Baron et al., JHEP **06**, 111 (2010), arXiv:1004.5284 [hep-lat].
 - [25] R. Baron et al. (ETM), JHEP **08**, 097 (2010), arXiv:0911.5061 [hep-lat].
 - [26] C. Alexandrou et al. (European Twisted Mass), Phys. Rev. **D78**, 014509 (2008), arXiv:0803.3190 [hep-lat].
 - [27] C. Alexandrou, R. Baron, J. Carbonell, V. Drach, P. Guichon, K. Jansen, T. Korzec, and O. Pene (ETM), Phys. Rev. **D80**, 114503 (2009), arXiv:0910.2419 [hep-lat].
 - [28] K. Jansen, A. Shindler, C. Urbach, and I. Wetzel (XLF), Phys. Lett. **B586**, 432 (2004), arXiv:hep-lat/0312013 [hep-lat].
 - [29] B. Blossier, P. Dimopoulos, R. Frezzotti, V. Lubicz, M. Petschlies, F. Sanfilippo, S. Simula, and C. Tarantino (ETM), Phys. Rev. **D82**, 114513 (2010), arXiv:1010.3659 [hep-lat].
 - [30] R. Frezzotti, S. Sint, and P. Weisz (ALPHA), JHEP **07**, 048 (2001), arXiv:hep-lat/0104014 [hep-lat].
 - [31] D. Becirevic and F. Sanfilippo, JHEP **01**, 028 (2013), arXiv:1206.1445 [hep-lat].
 - [32] K. Osterwalder and E. Seiler, Annals Phys. **110**, 440 (1978).
 - [33] P. F. Bedaque, Phys. Lett. **B593**, 82 (2004), arXiv:nucl-th/0402051 [nucl-th].
 - [34] C. T. Sachrajda and G. Villadoro, Phys. Lett. **B609**, 73 (2005), arXiv:hep-lat/0411033 [hep-lat].
 - [35] S. Ozaki and S. Sasaki, Phys. Rev. **D87**, 014506 (2013), arXiv:1211.5512 [hep-lat].
 - [36] B. B. Brandt, S. Capitani, M. Della Morte, D. Djukanovic, J. Gegelia, G. von Hippel, A. Jutner, B. Knippschild, H. B. Meyer, and H. Wittig, Eur. Phys. J. ST **198**, 79 (2011), arXiv:1106.1554 [hep-lat].
 - [37] K. A. Olive et al. (Particle Data Group), Chin. Phys. **C38**, 090001 (2014).
 - [38] C. C. Zhang et al. (Belle), Phys. Rev. **D86**, 052002 (2012), arXiv:1206.5087 [hep-ex].